

## Article

# Design of Third-Order Dispersion Compensation for the SG PW Laser System Using a Birefringent Crystal

Dawei Li <sup>1,2</sup>, Tao Wang <sup>3,\*</sup>, Xiaolei Yin <sup>4</sup>, Jiamei Li <sup>1,2</sup>, Hui Yu <sup>1,2</sup>, Li Wang <sup>1</sup>, Xingqiang Lu <sup>1,\*</sup> and Guang Xu <sup>1</sup>

<sup>1</sup> Key Laboratory of High Power Laser and Physics, Shanghai Institute of Optics and Fine Mechanics, Chinese Academy of Sciences, Shanghai 201800, China; lidw135@siom.ac.cn (D.L.); jmli@siom.ac.cn (J.L.); huiyu@siom.ac.cn (H.Y.); wl@siom.ac.cn (L.W.); xuguang@siom.ac.cn (G.X.)

<sup>2</sup> Center of Materials Science and Optoelectronics Engineering, University of Chinese Academy of Sciences, Beijing 100049, China

<sup>3</sup> Shanghai Institute of Laser Plasma, Chinese Academy of Engineering Physics, Shanghai 201800, China

<sup>4</sup> School of Sciences, Changzhou Institute of Technology, Changzhou 213032, China; yinxl@czust.edu.cn

\* Correspondence: twang@siom.ac.cn (T.W.); xinqianglu@siom.ac.cn (X.L.); Tel.: +86-021-6991-8723 (T.W.); +86-021-6991-8292 (X.L.)

**Abstract:** This study aims to update the existing SG PW laser system and improve the temporal contrast and shape fidelity of a compressed pulse with a 150 fs level for multi-PW (5–10 PW). The design of third-order dispersion (TOD) compensation via a birefringent crystal was studied through numerical simulations and experiments. The dispersions introduced by the birefringent crystal were calculated using the Jones matrix element by changing the in-plane rotation angle  $\phi$ , thickness  $d$ , incident angle  $\theta$ , and temperature  $T$ , while also considering the transmission spectral bandwidth. The group-velocity dispersion (GVD), TOD, and fourth-order dispersion (FOD) of the existing SG PW laser system and its influence on the compressed pulse with different pulse durations were analyzed. The results suggest that a TOD of  $1.3 \times 10^6 \text{ fs}^3$  needs to compensate for the multi-PW design. The compensation scheme is designed using a quartz crystal of  $d = 6.5 \text{ mm}$ ,  $\theta = 90^\circ$ ,  $\phi = 17^\circ$ , and  $T = 21^\circ \text{C}$ , corresponding to the thickness, inclination angle, in-plane rotation angle, and temperature, respectively. Furthermore, we show a principle-proof experiment offline and measure the GVD and TOD by the Wizzler, which is based on theoretical simulations. These results can be applied to independently and continuously control the TOD of short-pulse laser systems.

**Keywords:** third-order dispersion compensation; birefringent crystal; SG PW laser system; temporal contrast; shape fidelity; multi-PW laser



**Citation:** Li, D.; Wang, T.; Yin, X.; Li, J.; Yu, H.; Wang, L.; Lu, X.; Xu, G. Design of Third-Order Dispersion Compensation for the SG PW Laser System Using a Birefringent Crystal. *Appl. Sci.* **2022**, *12*, 4078. <https://doi.org/10.3390/app12084078>

Academic Editor: Luca Labate

Received: 5 March 2022

Accepted: 14 April 2022

Published: 18 April 2022

**Publisher's Note:** MDPI stays neutral with regard to jurisdictional claims in published maps and institutional affiliations.



**Copyright:** © 2022 by the authors. Licensee MDPI, Basel, Switzerland. This article is an open access article distributed under the terms and conditions of the Creative Commons Attribution (CC BY) license (<https://creativecommons.org/licenses/by/4.0/>).

## 1. Introduction

Owing to the development of chirped pulse amplification (CPA) technology, high-energy and short-pulse laser facilities have recently attracted considerable interest for their physical applications [1–5]. Designing the stretcher and compressor and controlling the dispersions to achieve the shortest pulse duration is an essential problem in CPA. The group-velocity dispersion (GVD) caused by the transmission and amplifier mediums can be compensated by stretcher or compressor adjustment in the laser system; however, residual third-order dispersion (TOD) and fourth-order dispersion (FOD) are still important, especially for shorter pulses, which can influence the intensity contrast and shape fidelity of the compressed pulse. Therefore, many research groups have studied the control and compensation of high-order dispersions by introducing different schemes [6–16].

As a significant pioneer devoted to high-power laser technology research in China, the National Laboratory on High Power Laser and Physics (NLHPLP) has built many laser facilities, formally named the ‘Shen Guang’ (SG) series facilities after 1986 [17]. Therefore, the kilojoule-class Petawatt (PW) laser system is called the SG PW laser here. The SG PW laser system [18] uses hybrid CPA technology combining OPCPA and Nd: glass CPA to

achieve maximum energy of 1 kJ with a compressed pulse duration of approximately 1 ps, and the focused intensity is up to  $10^{20}$  W/cm<sup>2</sup> with a diameter of 20.8  $\mu$ m in 50% cycle, which were achieved in 2016. The SG PW laser is generally used to heat and generate energetic protons in various physical experiments, such as fast ignition, indirect drive physics, laboratory astrophysics, and high energy density physics. Furthermore, to meet the demand for further physical applications, the design of a multi-PW (5–10 PW) with a pulse duration of 150 fs at 1053 nm has recently been approved, which is similar to the aforementioned design [19–21] and can be updated from the existing SG PW laser system. The amplified pulse, stretched by the Offner stretcher [22], is recompressed with a four-grating compressor, which can cancel out the GVD introduced by the transmission and amplifier materials in the system simultaneously. However, the residual TOD and FOD can influence the intensity contrast and shape fidelity of the compressed pulse when the pulse duration decreases and hence require compensation. The methods of compensating for the TOD include object-image-grating self-tiling [6] and fiber [8–10,12,16], prism pair [13], and acousto-optic programmable dispersion filter (AOPDF) [14,15], which are limited by the damage threshold, apertures, and low transmission, and are mainly set in a position of relatively low energy before amplification, leading to the lower energy of the input pulses. On the other hand, the hybrid gratings scheme [7] and Gires–Tournois interferometer (GTI) mirrors [11] can be used to compensate for the TOD with a large aperture but it is difficult to process and is not convenient to adjust. Therefore, finding a method to support high energy with a large aperture and convenient operation is required, especially for the TOD compensation of a multi-PW design based on the existing SG PW laser system. Birefringent crystals have been widely used to achieve gain-narrow compensation in CPA amplifiers [23,24]; however, to the best of our knowledge, few applications and considerations of birefringent crystals have been reported in detail for the introduced spectral phase and dispersions, especially in the experiment. Therefore, we investigated the design of TOD compensation for the SG PW laser system using a birefringent crystal. The remainder of this paper is organized as follows.

First, the numerical model for the dispersions introduced by the birefringent crystal is presented in Section 2. Second, the residual TOD and FOD for the existing SG PW laser system for different pulse durations are calculated, and their influence on the contrast is analyzed in Section 3.1. Third, in Section 3.2, the dispersion introduced by the birefringent crystal is studied to vary the in-plane rotation angle  $\phi$ , thickness  $d$ , incident angle  $\theta$ , and temperature  $T$ , while considering the transmission spectral bandwidth. Furthermore, a scheme of  $1.3 \times 10^6$  fs<sup>3</sup> TOD compensation for the SG PW laser system is designed using a quartz birefringent crystal with  $d = 6.5$  mm,  $\theta = 90^\circ$ ,  $\phi = 17^\circ$ , and  $T = 21$  °C. Finally, the dispersions of GVD and TOD introduced by the birefringent crystals are investigated offline using a Wizzler for a proof-principle experiment, as described in Section 3.3.

## 2. Numerical Method

A schematic for when a birefringent plate is used in dispersion compensation, which is similar to spectral modulation, is shown in Figure 1.  $\theta$  is the angle between the incident ray and the crystal surface, which denotes the inclination angle, and  $\phi$  is the angle between the crystal optical axis and the incident surface which denotes the in-plane rotation angle.

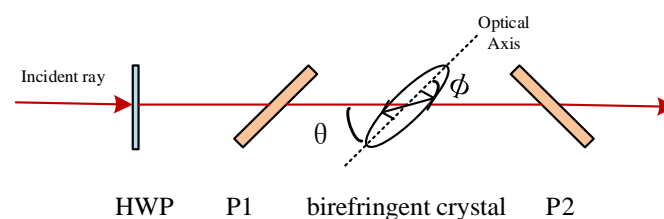


**Figure 1.** Schematic of the dispersion compensation based on the birefringent plate. P1, P2: Polarizers; HWP: Half-wave plate.

The electric field of the pulsed laser after the polarizer P2 can be described by  $E_{Out} = E_{In}m_{22}$ , where  $m_{22}$  is the Jones matrix element of the birefringent plate [25,26], which can be expressed as follows:

$$M_b = \left(1 - \frac{\cos^2 \Phi \sin^2 \theta}{qn_e^2}\right) \times \begin{bmatrix} \left(1 - \frac{\sin^2 \theta}{qn_e^2}\right) \cos^2 \Phi \exp(i\delta_e) + \sin^2 \Phi \exp(i\delta_o) & \left(1 - \frac{\sin^2 \theta}{qn_e^2}\right)^{\frac{1}{2}} \sin \Phi \cos \Phi [\exp(i\delta_e) - \exp(i\delta_o)] \\ \left(1 - \frac{\sin^2 \theta}{qn_e^2}\right)^{\frac{1}{2}} \sin \Phi \cos \Phi [\exp(i\delta_e) - \exp(i\delta_o)] & \left(1 - \frac{\sin^2 \theta}{qn_e^2}\right) \cos^2 \Phi \exp(i\delta_o) + \sin^2 \Phi \exp(i\delta_e) \end{bmatrix} \quad (1)$$

where

$$q = 1 - \left(\frac{1}{n_o^2} - \frac{1}{n_e^2}\right) \sin^2 \theta_i \cos^2 \phi \quad (2)$$

$$\delta_o = \frac{2\pi}{\lambda} d \frac{n_o}{\left(1 - \frac{\sin^2 \theta_i}{n_o^2}\right)^{1/2}} \quad (3)$$

and

$$\delta_e = \frac{2\pi}{\lambda} d \left[ n_e \left(1 - \frac{\sin^2 \theta_i \sin^2 \phi}{n_e^2} - \frac{\sin^2 \theta_i \cos^2 \phi}{n_o^2}\right)^{1/2} - n_o \left(1 - \frac{\sin^2 \theta_i}{n_o^2}\right) + \frac{n_o}{\left(1 - \frac{\sin^2 \theta_i}{n_o^2}\right)^{1/2}} \right] \quad (4)$$

The thickness  $d$  is related to temperature according to

$$d(T) = d_0[1 + \alpha(T - T_0)] \quad (5)$$

A quartz birefringent crystal was used in this study. The expansion coefficient of quartz was  $a = 13.3667 \times 10^{-6}$  at 18 °C [27]. The refractive indices depend on both wavelength and temperature. For quartz, the following empirical formula was used for the principal refractive indices:

$$n_i = [t_i + s_i(\lambda - \lambda_{2i})](T_0 - T) + \sqrt{m_i + m_{1i}\lambda^2 / (\lambda^2 - \lambda_{1i}^2) - k_i\lambda^2} \quad (6)$$

where the subscript  $i$  corresponds to o and e, for ordinary and extraordinary, respectively,  $\lambda$  is the wavelength,  $T$  is the temperature, and  $t_i$ ,  $s_i$ ,  $m_i$ , and  $k_i$  are parameters that are evaluated from the literature [27].

The intensity and phase of the output field were obtained using  $I_{Out} = E_{Out}E_{Out}^*$  and  $\varphi(\omega) = \tan^{-1}[\text{Im}(E_{Out})/\text{Re}(E_{Out})]$ . The dispersions introduced by the birefringent plate can then be described as

$$\varphi(\omega) = \varphi_0 + \varphi_1(\omega - \omega_0) + \frac{1}{2}\varphi_2(\omega - \omega_0)^2 + \frac{1}{6}\varphi_3(\omega - \omega_0)^3 + \dots \quad (7)$$

where  $\omega$  and  $\omega_0$  are the laser and center frequencies, respectively.  $\varphi_0$  is the absolute phase,  $\varphi_1$  is the group delay (GD), and  $\varphi_2$  and  $\varphi_3$  are GVD and TOD, respectively. The dispersion of each order introduced by the crystal can be controlled by the thickness  $d$ , inclination angle  $\theta$ , in-plane rotation angle  $\phi$ , and temperature  $T$ .

According to Equations (1)–(4), the center wavelength of transmission and dispersions can be adjusted by a combination of length, angle, and temperature, which is a periodic function and can be precisely controlled by tuning the temperature of the crystal, especially when the length is fixed after processing.

### 3. Results and Discussion

#### 3.1. Residual TOD and FOD and Influence on the Multi-PW Design

As previously mentioned, in the process of chirped pulse amplification, the stretcher, compressor, transmission materials, and amplifier media can introduce different magnitude levels of GVD, TOD, and FOD. While the pulse can be compressed to the near Fourier transform limit (FTL) after GVD is completely compensated, residual high-order dispersions are still present. As shown in Figure 2, the existing SG PW laser system [18] can afford a compressed pulse duration of 1 ps with an energy level of 1 kJ and a bandwidth of approximately 3 nm, which is mainly caused by the gain narrowing effect and system B integral of 1.78. A multi-PW with a 150 fs level and energy of over 0.75 kJ can be achieved by changing the oscillator to a pulse duration of 80 fs, updating the stretcher and compressor, together with a bandwidth extension achieved by spectral shaping after OPCPA with an energy of 1 J, which is similar to [28]. The bandwidth can be extended after compensation for the gain-narrowing effect, which can also decrease the B integral to less than 1 and improve the amplified pulse energy to over 0.75 kJ simultaneously. However, as the pulse duration becomes shorter, the residual high-order dispersions of the TOD and FOD may significantly influence the contrast and pulse shape.

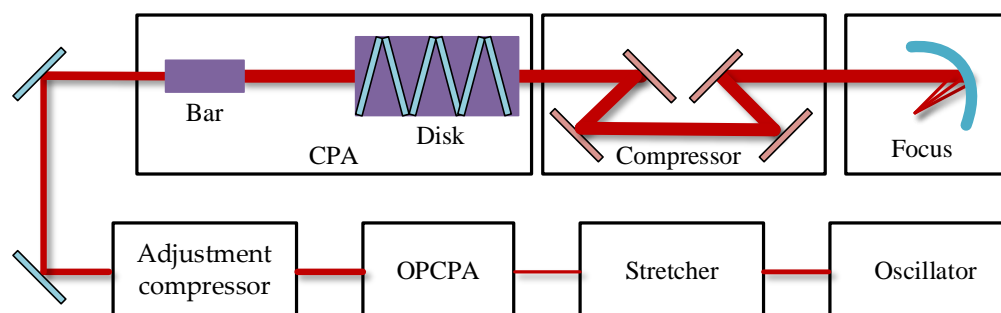


**Figure 2.** Block diagram of the existing SG PW laser system.

For the existing SG PW laser system, a 180 fs hyperbolic secant pulse shape centered at 1053 nm from the oscillator is stretched to 3.3 ns by an eight-pass single-grating Offner stretcher to suit the 6 ns pulse duration of the OPCPA pump. It is then amplified to 2 kJ by the Nd:glass amplifier chain and finally compressed by a four-grating single-pass compressor. In addition, the total length of the Nd:glass and BK7 lenses in the system are approximately 3.35 m and 0.36 m [6]. The GVD can be adjusted using an adjustment compressor set after the OPCPA, which can control the pulse duration from the FTL to 30 ps.

To confirm the criterion for high-order dispersion compensation, the residual TOD and FOD for the multi-PW design are first analyzed, and then the influences of the dispersions on the compressed pulse are illustrated. As can be seen in Figure 3, the absolute values of the GVD, TOD, and FOD for pulse durations of 180 fs (Figure 3a–c) and 80 fs (Figure 3d–f) are simulated using the Offner stretcher and compressor design [29–31] without considering the dispersions of transmission materials and amplifier mediums, together with the differences in dispersion between the stretcher and compressor. The pulse is stretched to 3.3 ns and compressed to the FTL in the simulation. The stretcher affords a positive dispersion of the GVD, and the compressor affords negative values. As illustrated in Figure 3, the GVD introduced by the stretcher and compressor coincide and can be canceled at a central wavelength of 1053 nm, but the residual TOD and FOD are  $6 \times 10^3 \text{ fs}^3$  and  $-3.6 \times 10^8 \text{ fs}^4$  for a pulse duration of 180 fs, and  $1.2 \times 10^2 \text{ fs}^3$  and  $-8 \times 10^6 \text{ fs}^4$  for a pulse duration of 80 fs. These are mainly caused by the pulse with a longer duration according to a narrower bandwidth, which demands a larger GVD to achieve the same stretched pulse duration of 3.3 ns, and needs to pass through a longer optical path in the stretcher and compressor, thereby introducing more aberrations for the TOD and FOD. The analysis dispersion results are consistent with implementing a stretcher and compressor for the SG PW laser

with a seed pulse duration of 180 fs. They can also provide a design basis for upgrading to multi-PW.

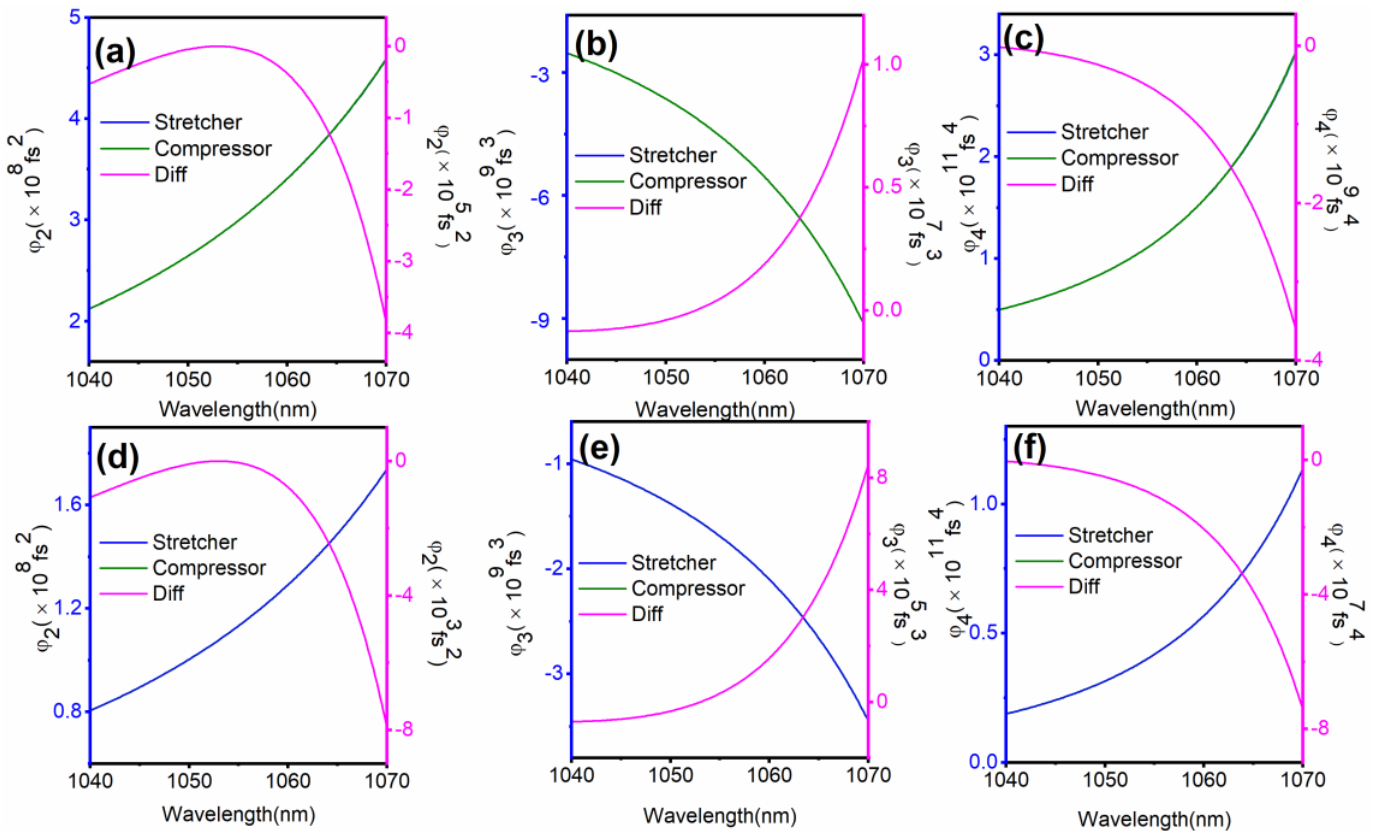


**Figure 3.** Absolute value of the GVD, TOD, and FOD for pulse durations of 180 fs and 80 fs, which are stretched to 3.3 ns and compressed to FTL, together with the differences of dispersion between stretcher and compressor. (a) The GVD and difference for the pulse duration of 180 fs; (b) the TOD and difference for the pulse duration of 180 fs; (c) the FOD and difference for the pulse duration of 180 fs; (d–f) are similar as above for the pulse duration of 80 fs.

Compared with the pulse duration of 180 fs, the residual TOD and FOD are small in the multi-PW design with a seed pulse duration of 80 fs. However, to compensate for the dispersion caused by the transmission materials and amplifier mediums [6], in which the GVD, TOD, and FOD are approximately  $8.8 \times 10^4 \text{ fs}^2$ ,  $1.54 \times 10^5 \text{ fs}^3$ , and  $-1.69 \times 10^5 \text{ fs}^4$ . An adjustment compressor is used to compensate for the above GVD; however, this process can introduce extra TOD and FOD simultaneously. The change in the distance for adjusting the compressor gratings, GVD, TOD, and FOD for pulse durations of 180 fs (dotted line in blue) and 80 fs (solid in black line) with adjustable pulse durations are shown in Figure 4a–d. To achieve an FTL compressed pulse, the adjusted compressor needs to afford a GVD of  $-8.8 \times 10^4 \text{ fs}^2$  and introduce an additional but the same TOD of  $1.3 \times 10^6 \text{ fs}^3$  and FOD of  $-3 \times 10^7 \text{ fs}^4$  simultaneously. After compensating for the GVD of the transmission materials, the final TOD and FOD for the existing SG PW laser system are  $1.3 \times 10^6 \text{ fs}^3$  and  $-3.9 \times 10^8 \text{ fs}^4$  for a pulse duration of 180 fs and  $1.3 \times 10^6 \text{ fs}^3$  and  $-3.8 \times 10^7 \text{ fs}^4$  for a pulse duration of 80 fs. The values agree with the implementation of pulse duration controlled by the adjustment compressor in the SG PW laser and can provide a basis for the multi-PW design.

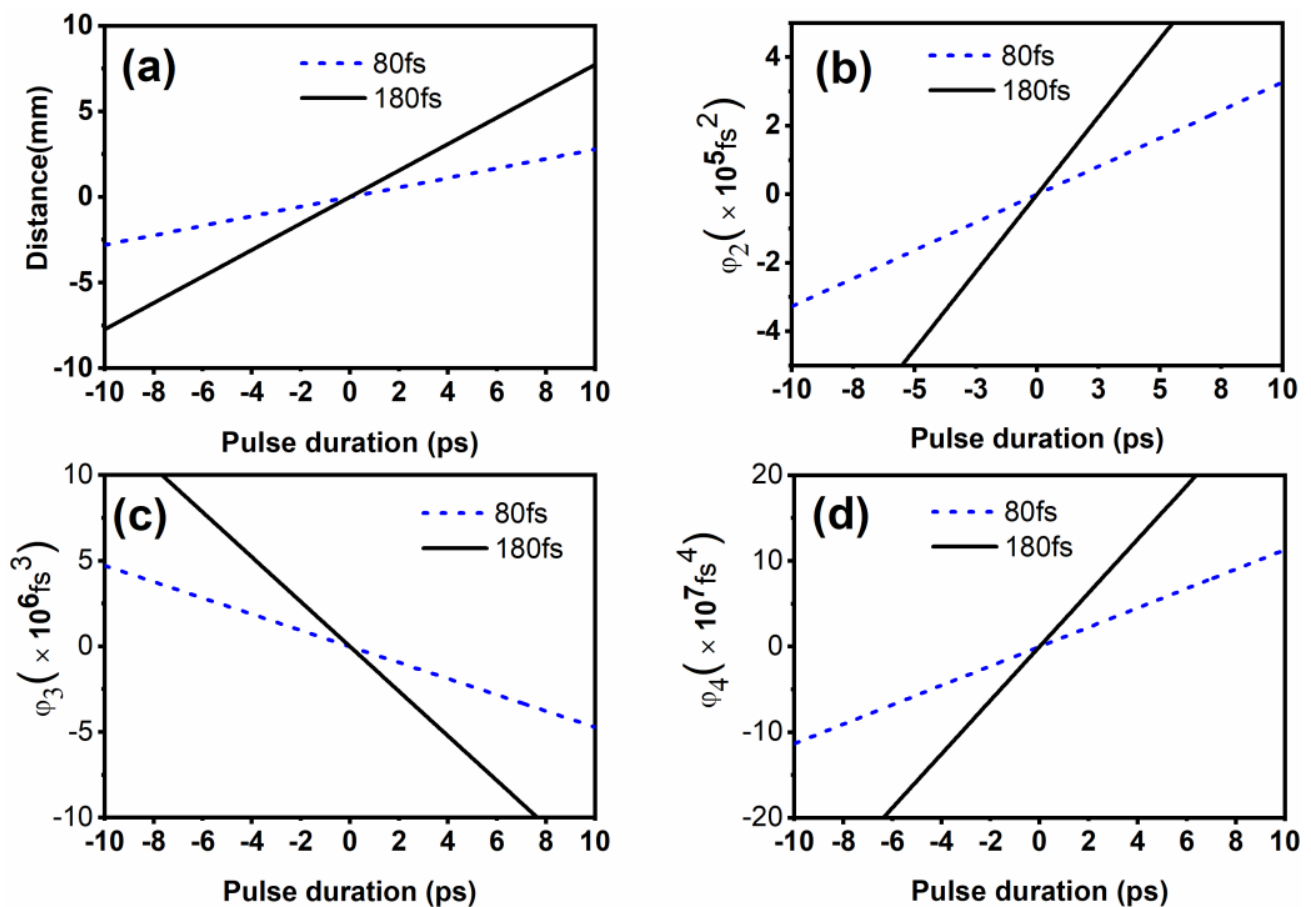


**Figure 4.** Distance of adjustment compressor gratings, the GVD, TOD, and FOD change with pulse durations by the adjustable compressor for the pulse durations of 180 fs (solid black lines) and 80 fs (dotted blue lines), respectively. (a) Distance; (b) GVD; (c) TOD; (d) FOD.

To illustrate the influence of the residual high-order dispersions of the TOD and FOD on the contrast and pulse shapes, Figure 5a shows the intensity contrast for bandwidths of 3 nm, 5 nm, and 7 nm with the TOD of  $1.3 \times 10^6 \text{ fs}^3$  and FOD of  $-3.9 \times 10^8 \text{ fs}^4$ , according to the gain narrowing effect and compressed FTL pulse durations of 388 fs, 233 fs, and 166 fs, respectively. A comparison of the contrast with the compensation of TOD and the residual FOD is shown in Figure 5b; the B integral is neglected in the simulation. Similarly, Figure 5c shows the intensity contrast for bandwidths of 7 nm, 11 nm, and 15 nm, according to the compressed FTL pulse durations of 388 fs, 105 fs, and 77 fs, respectively, and includes the TOD of  $1.3 \times 10^6 \text{ fs}^3$  and FOD of  $-3.8 \times 10^7 \text{ fs}^4$ ; only the residual FOD is shown in Figure 5d. From the comparison results of Figure 5, we can see that the residual TOD and FOD had no significant effect on the contrast for the existing SG PW laser with a bandwidth of 3 nm after gain narrowing [18], but high-order dispersion should be considered if the pulse bandwidth is broadened and compressed to the FTL. The simulated result for the bandwidth of 3 nm can afford the measured contrast of  $10^{-8}$ , by which there is no additional TOD dispersion adjustment in the SG PW laser. However, when the pulse bandwidth is broadened to over 7 nm, and the duration is shorter than 150 fs in the multi-PW design, the TOD can significantly distort the pulse shape and the pulse is no longer symmetric, which can cause the peak power of the pulse to decrease. Therefore, the TOD must be compensated, but the FOD is negligible. Furthermore, when the pulse duration is less than 100 fs, the FOD should be considered to further improve the intensity contrast, which is consistent with the results obtained in [32].

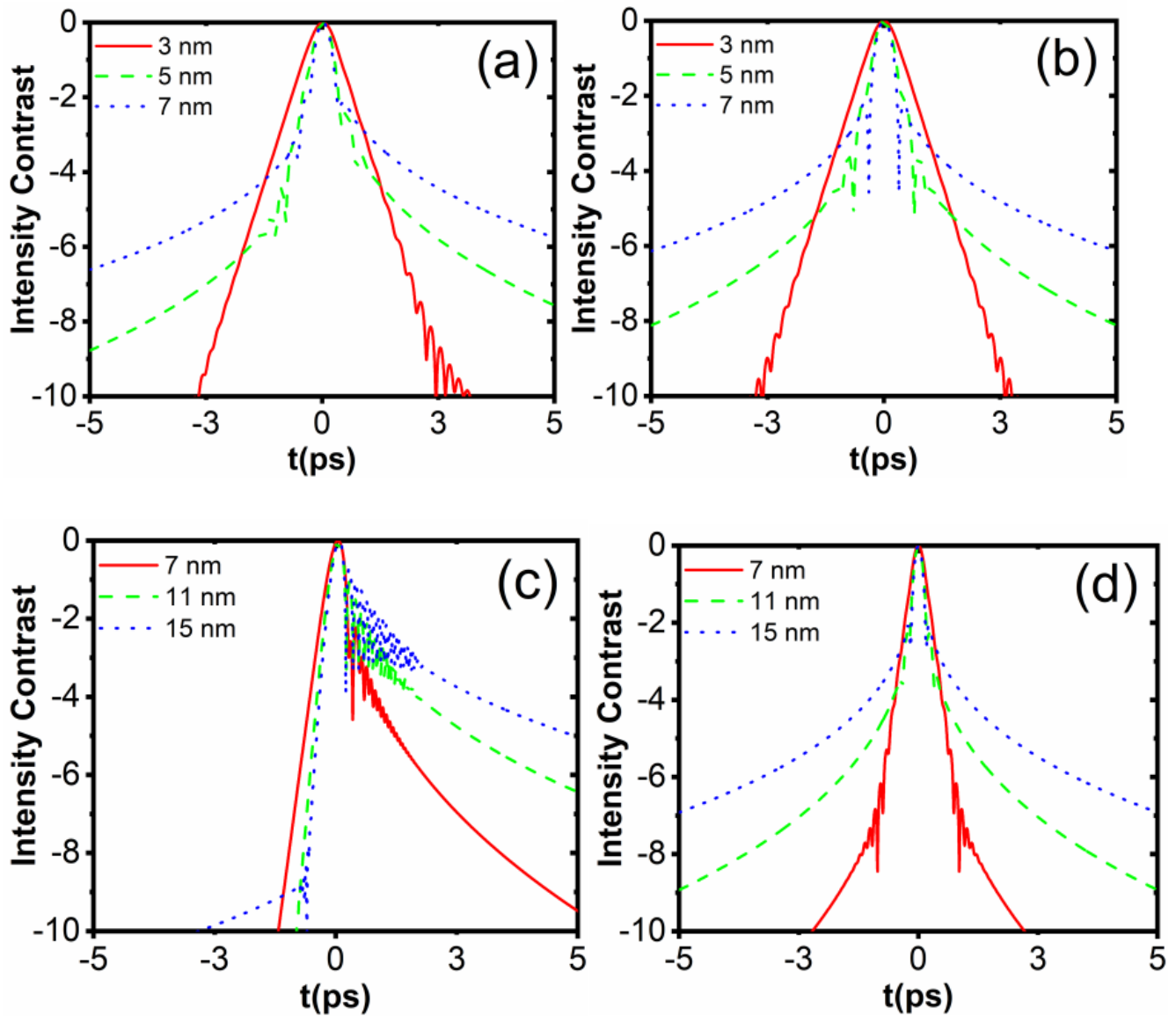


**Figure 5.** (a) Intensity contrast for bandwidths of 3 nm, 5 nm, and 7 nm, which includes the TOD of  $1.3 \times 10^6 \text{ fs}^3$  and FOD of  $-3.9 \times 10^8 \text{ fs}^4$ ; (b) the contrast only with the FOD, with other parameters the same as in (a); (c) the contrast for bandwidths of 7 nm, 11 nm, and 15 nm including the TOD of  $1.3 \times 10^6 \text{ fs}^3$  and FOD of  $-3.8 \times 10^7 \text{ fs}^4$ ; (d) the contrast only considering the FOD, with other parameters the same as in (c).

### 3.2. Design of TOD Compensation Using the Birefringent Plate

Here, we aim to compensate the TOD of  $1.3 \times 10^6 \text{ fs}^3$  for the multi-PW with a 150-fs level design. As detailed in Figure 6a, we first analyze the variation of the maximum amplitude of TOD and free-spectral range (FSR) with the length of the birefringent plate using Equations (1)–(7), where the parameters are  $\theta = 90^\circ$ ,  $\phi = 17^\circ$ , and  $T = 21^\circ\text{C}$ . Similar to the GTI, the maximum amplitude of the TOD increased, but the FSR decreased with increasing plate length. Figure 6b shows the GVD and TOD change with  $\phi$ , in which the length of the plate is 6.5 mm, and the other parameters are the same as in Figure 6a. In addition, the TOD can be adjusted from positive to negative with the scope of  $\pm 2 \times 10^6 \text{ fs}^3$ , which can compensate for the residual TOD of  $1.3 \times 10^6 \text{ fs}^3$  for the multi-PW design when  $\phi$  is set to  $17^\circ$ . Furthermore, the GVD is small and can be neglected. Additionally, the transmission, GVD, and TOD curves changing with wavelength are also shown in Figure 6c,d, respectively, when the birefringent plate is set to the compensation TOD of  $1.3 \times 10^6 \text{ fs}^3$ .

As shown above, the dispersion scheme can support the bandwidth of approximately 7 nm and the TOD of  $1.3 \times 10^6 \text{ fs}^3$ , which can be used to compensate for the demanded TOD for the multi-PW design. In addition, similar to the results of crystal cascade increasing the bandwidth [33], we observe from Figure 6 that the birefringent crystal can also be cascade designed to afford larger bandwidth with the same TOD simultaneously in the dispersion compensation. From the results, the residual TOD for multi-PW design can be compensated by choosing the thickness and controlling the inclination angle, the in-plane angle, and the temperature of the birefringent plate independently.

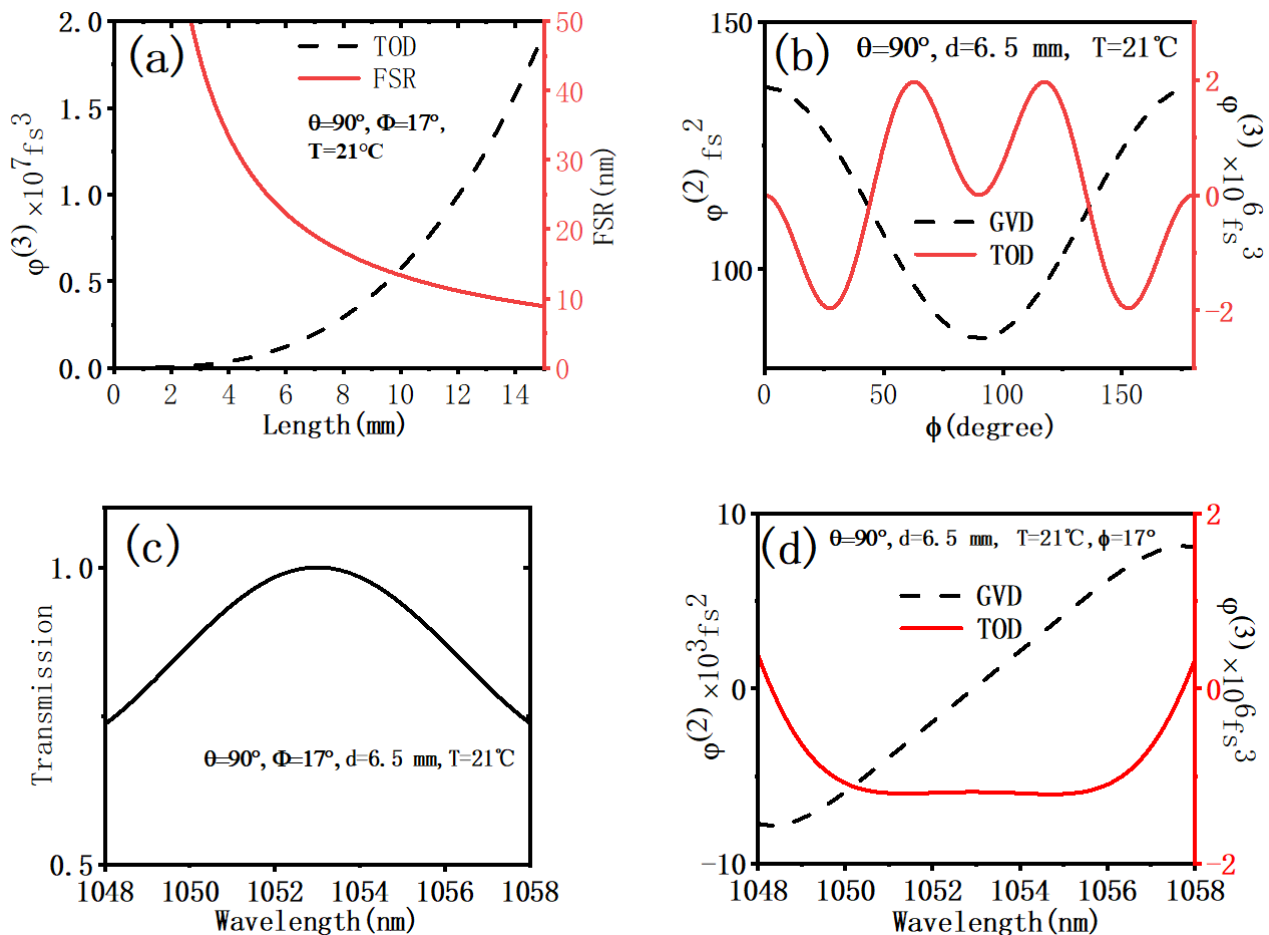


**Figure 6.** (a) Maximum amplitude of TOD and FSR changing with the length of the birefringent plate; (b) The GVD and TOD change with  $\phi$ , in which the length of the plate is 6.5 mm; (c) The transmission curve for TOD compensation; (d) The GVD and TOD curves changing with wavelength for the TOD compensation parameters.

### 3.3. Experiment

Figure 7 shows the schematic diagram of the principle-proof experiment for TOD control using a quartz birefringent crystal, according to the arrangement in Figure 1. The spectral phase of short pulse is generally measured by commercial equipment of Frequency-resolved optical gating or Wizzler. However, to measure the GVD and TOD directly with high precision, we used the Wizzler (Wizzler-1030) in the experiment. Considering the Wizzler needs the energy of several microjoules and a pulse duration of nearly FTL, the oscillator is not suitable anymore. Therefore, we used a laser source (Origami-10XP) with a pulse duration of 400 fs (FTL = 280 fs), 100 kHz, and an energy of 30  $\mu\text{J}$  at 1039 nm to satisfy the energy and pulse duration demand for the dispersion measurement. The light from the laser passes through the quartz birefringent crystal and polarizers of P1 and P2 using the reflecting mirrors M1 and M2 and is finally directed into the Wizzler. The energy

of input Wizzler can be adjusted by half waveplate (HWP) and P1. It is worth noting that the laser has inherent GVD and TOD caused by a non-FTL compressed pulse and the seed of a fiber oscillator. To distinguish the GVD and TOD clearly in the experiment, the quartz of length 11.98 mm was used with an environmental temperature of 25 °C, the angle  $\theta$  was set to 86° to reduce the effect of reflected light on the laser, and the angle  $\phi$  can be varied in plane by a rotation adjustment mechanism.

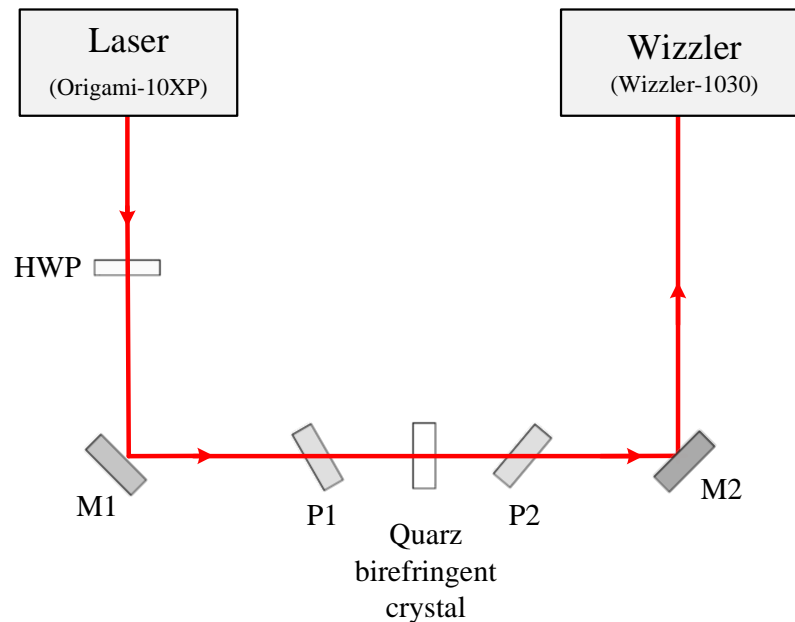


**Figure 7.** Schematic diagram of principle-proof experiment for dispersion control, which uses a quartz birefringent crystal and measured by Wizzler; HWP is the half waveplate; M1 and M2 are reflector mirrors; P1 and P2 are polarizers.

The changes in GVD and TOD with  $\phi$  were measured with Wizzler, and the results are shown in Figure 8a,b, in which the measured GVD and TOD introduced by the quartz crystal are obtained using the difference between the measured values and the inherent dispersion of the laser. The GVD and TOD periodically change with the angle  $\phi$ , and the non-symmetrical amplitudes of the peaks and valleys are caused by  $\theta$  not being equal to 90°. To the best of our knowledge, the experimental results for the GVD and TOD caused by birefringent crystals are first demonstrated here. The differences between the experiments and simulations mainly caused the residual GVD of  $-6 \times 10^4 \text{ fs}^2$  and the TOD of  $5 \times 10^6 \text{ fs}^3$  from the laser, resulting in more deviation, especially when measuring the peaks and valleys for TOD. Figure 8c shows the spectrum and phase with a GVD of  $-6 \times 10^4 \text{ fs}^2$  and TOD of  $5 \times 10^6 \text{ fs}^3$  from the initial laser without inserting quartz, and Figure 8d shows the GVD of  $-8 \times 10^4 \text{ fs}^2$  and TOD of  $-1.3 \times 10^7 \text{ fs}^3$  when using the birefringent quartz crystal, according to the valleys in Figure 8b. In addition, the spectrum in Figure 8d is modulated mainly by the longer crystal, which can limit the FSR.

Furthermore, Compared to the case of spectral intensity shaping by using the birefringent crystal, the initial position of  $\phi = 0^\circ$  should be confirmed when using the crystal for dispersion compensation. The thickness and temperature should also be precisely processed and controlled to fix the maximum TOD simultaneously. The results suggest that the birefringent crystal can independently and continuously control the TOD through  $\phi$  and can be used to compensate for the TOD in the multi-PW design.

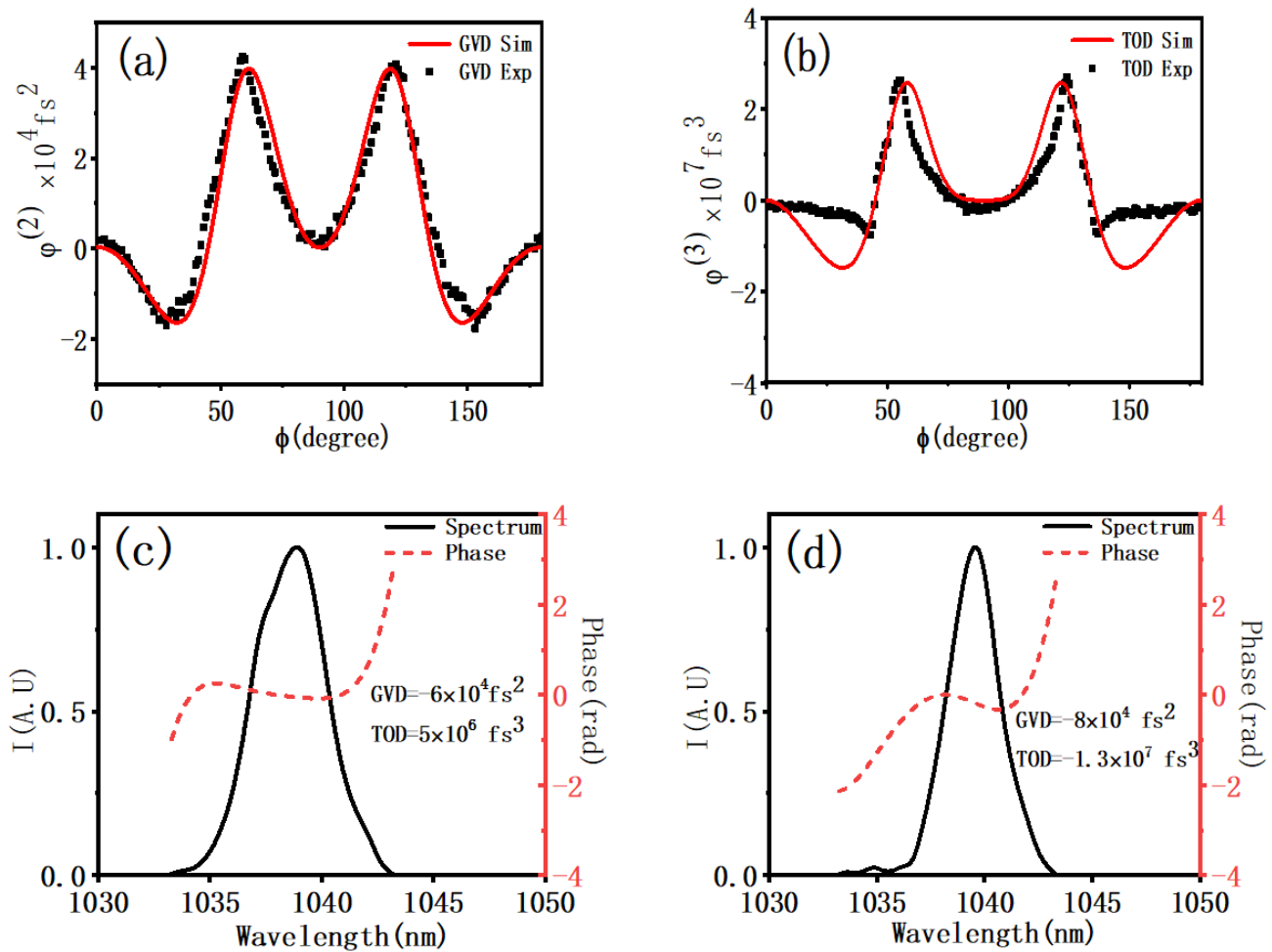


**Figure 8.** (a) Experimental measurement results of GVD represented by the dotted black line, compared with simulated results shown by the solid red line; (b) the measured and simulated TOD; (c) the initial spectral and phase measurement with the residual GVD of  $-6 \times 10^4 \text{ fs}^2$  and TOD of  $5 \times 10^6 \text{ fs}^3$  from the laser without inserting quartz; (d) the spectral and phase with the GVD of  $-8 \times 10^4 \text{ fs}^2$  and the TOD of  $-1.3 \times 10^7 \text{ fs}^3$ , according to the valleys in Figure (b).

#### 4. Conclusions

Motivated by the promising design for a multi-PW laser with a 150-fs level based on the existing SG PW laser system, the temporal contrast and shape fidelity of the compressed pulse influenced by TOD should be compensated. Hence, finding a method to support increased energy with a large aperture, highly efficient transmission, and convenient operation is required. Therefore, a TOD compensation scheme using a temperature-tuning birefringent crystal is proposed in this paper. The GVD, TOD, and FOD of the existing SG PW laser system and their influence on the compressed pulse with different bandwidths are analyzed to provide an evaluation basis for compensating dispersions of the TOD and FOD. The results indicated that TOD compensation is necessary for a pulse duration of 150 fs. The TOD introduced by the quartz birefringent crystal was calculated, and the compensation scheme for the TOD of  $1.3 \times 10^6 \text{ fs}^3$  was designed using a quartz crystal. Furthermore, a principle-proof experiment was investigated offline to measure the GVD and TOD by a Wizzler, which is based on theoretical simulations. These results provide a feasible method for controlling and compensating the TOD with a temperature-regulated birefringent crystal, which to the best of our knowledge, is achieved for the first time. In addition, they are important for supporting updates of the multi-PW (5–10 PW) at the 150-fs level.

The large-scale laser system has higher residual TOD and needs a thicker birefringent crystal to compensate. The FSR may be affected but can be controlled by cascaded crystals. Further work is planned to use this scheme in an online laser system by using the designed parameters and judging the dispersions and FSR in detail. Furthermore, the residual TOD is lower for small-scale laser systems, such as high average power fiber lasers with a short pulse. The method can afford more FSR and will be more beneficial and convenient for achieving high time-domain fidelity for the compressed pulse after TOD compensation.

**Author Contributions:** Conceptualization, D.L., T.W. and G.X.; Data curation, D.L. and G.X.; Funding acquisition, X.L. and G.X.; Investigation, H.Y. and J.L.; Methodology, D.L. and L.W.; Project administration, X.L. and G.X.; Software, X.Y. and X.L.; Supervision, T.W.; Validation, L.W. and X.Y.; Visualization, D.L.; Writing—original draft, D.L.; Writing—review and editing, X.Y. and L.W. All authors have read and agreed to the published version of the manuscript.

**Funding:** This research was funded by the International Partnership Program of the Chinese Academy of Sciences (grant number 181231KYSB20170022), and Fundamental Research Project of Changzhou Science and Technology (grant number CJ20200029).

**Institutional Review Board Statement:** Not applicable.

**Informed Consent Statement:** Not applicable.

**Data Availability Statement:** All the data reported in this paper are presented in the main text. Any other data will be provided on request.

**Conflicts of Interest:** The authors declare no conflict of interest. The funders had no role in the study design, collection, analyses, or interpretation of data; writing of the manuscript; or decision to publish the results.

## References

1. Moses, E.I.; Lindl, J.D.; Spaeth, M.L.; Patterson, R.W.; Sawicki, R.H.; Atherton, L.J.; Baisden, P.A.; Lagin, L.J.; Larson, D.W.; MacGowan, B.J.; et al. Overview: Development of the National Ignition Facility and the Transition to a User Facility for the Ignition Campaign and High Energy Density Scientific Research. *Fusion Sci. Technol.* **2017**, *69*, 1–24. [[CrossRef](#)]
2. Galletti, M.; Oliveira, P.; Galimberti, M.; Ahmad, M.; Archipovaite, G.; Booth, N.; Dilworth, E.; Frackiewicz, A.; Winstone, T.; Musgrave, I.; et al. Ultra-broadband all-OPCPA petawatt facility fully based on LBO. *High Power Laser Sci. Eng.* **2020**, *8*, e31. [[CrossRef](#)]
3. Zhang, J.; Wang, W.M.; Yang, X.H.; Wu, D.; Ma, Y.Y.; Jiao, J.L.; Zhang, Z.; Wu, F.Y.; Yuan, X.H.; Li, Y.T.; et al. Double-cone ignition scheme for inertial confinement fusion. *Philos. Trans. R. Soc. London. Ser. A Math. Phys. Eng. Sci.* **2020**, *378*, 20200015. [[CrossRef](#)] [[PubMed](#)]
4. Mariscal, D.; Ma, T.; Wilks, S.C.; Kemp, A.J.; Williams, G.J.; Michel, P.; Chen, H.; Patel, P.K.; Remington, B.A.; Bowers, M.; et al. First demonstration of ARC-accelerated proton beams at the National Ignition Facility. *Phys. Plasmas* **2019**, *26*, 43110. [[CrossRef](#)]
5. Hornung, J.; Zobus, Y.; Boller, P.; Brabetz, C.; Eisenbarth, U.; Kuhl, T.; Major, Z.; Ohland, J.B.; Zepf, M.; Zielbauer, B.; et al. Enhancement of the laser-driven proton source at PHELIX. *High Power Laser Sci. Eng.* **2020**, *8*, e24. [[CrossRef](#)]
6. Li, Z.; Rao, D.; Leng, Y.; Chen, L.; Dai, Y. Third-order dispersion compensation for petawatt-level lasers employing object-image-grating self-tiling. *Quantum Electron.* **2015**, *45*, 891.
7. Zaouter, Y.; Papadopoulos, D.N.; Hanna, M.; Druon, F.; Cormier, E.; Georges, P. Third-order spectral phase compensation in parabolic pulse compression. *Opt. Express* **2007**, *15*, 9372. [[CrossRef](#)]
8. Marhic, M.E.; Kagi, N.; Chiang, T.K.; Kazovsky, L.G. Cancellation of third-order nonlinear effects in amplified fiber links by dispersion compensation, phase conjugation, and alternating dispersion. *Opt. Lett.* **1995**, *20*, 863. [[CrossRef](#)] [[PubMed](#)]
9. Liu, S.; Liu, X. Mutual compensation of the higher-order nonlinearity and the third-order dispersion. *Phys. Lett. A* **1997**, *225*, 67. [[CrossRef](#)]
10. Zhang, R.; Yang, X.; Cai, Y.; Hu, W.; Zhang, Z. Residual third-order dispersion compensation in femtosecond pulses transmission using a phase modulator. In Proceedings of the Optical Transmission, Switching, and Subsystems VI, Hangzhou, China, 26–30 October 2008; Volume 7136.
11. Niu, H.L.; Shen, W.D.; Li, C.S.; Zhang, Y.G.; Xie, C.; Yu, P.; Yuan, W.J.; Liu, B.W.; Hu, M.L.; Wang, Q.Y.; et al. Dispersive mirrors for high third-order dispersion compensation in femtosecond amplification fiber laser system. *Appl. Phys. B* **2012**, *108*, 609. [[CrossRef](#)]
12. Kane, S.; Squier, J. Grating Compensation of Third-Order Material Dispersion in the Normal Dispersion Regime: Sub-100-fs Chirped-Pulse Amplification Using a Fiber Stretcher and Grating-Pair Compressor. *IEEE JQE* **1995**, *31*, 2052. [[CrossRef](#)]
13. Yang, Q.; Xie, X.; Kang, J.; Zhu, H.; Guo, A.; Gao, Q. Independent and continuous third-order dispersion compensation using a pair of prisms. *High Power Laser Sci. Eng.* **2014**, *2*, e38. [[CrossRef](#)]

14. Verluise, F.; Laude, V.; Cheng, Z.; Spielmann, C.; Tournois, P. Amplitude and phase control of ultrashort pulses by use of an acousto-optic programmable dispersive filter: Pulse compression and shaping. *Opt. Lett.* **2000**, *25*, 575. [[CrossRef](#)] [[PubMed](#)]
15. Lureau, F.; Matras, G.; Chalus, O.; Derycke, C.; Morbieu, T.; Radier, C.; Casagrande, O.; Laux, S.; Ricaud, S.; Rey, G.; et al. High-energy hybrid femtosecond laser system demonstrating  $2 \times 10$  PW capability. *High Power Laser Sci. Eng.* **2020**, *8*, 8. [[CrossRef](#)]
16. Tsuda, H.; Okamoto, K.; Ishii, T.; Naganuma, K.; Inoue, Y.; Takenouchi, H.; Kurokawa, T. Second- and third-order dispersion compensator using a high-resolution arrayed-waveguide grating. *IEEE Photonics Technol. Lett.* **1999**, *11*, 569. [[CrossRef](#)]
17. Zhu, J.; Zhu, J.; Li, X.; Zhu, B.; Ma, W.; Lu, X.; Fan, W.; Liu, Z.; Zhou, S.; Xu, G.; et al. Status and development of high-power laser facilities at the NLHPLP. *High Power Laser Sci.* **2018**, *6*, 6. [[CrossRef](#)]
18. Xu, G.; Wang, T.; Li, Z.; Dai, Y.; Lin, Z.; Gu, Y.; Zhu, J. 1 kJ Petawatt Laser System for SG-II-U Program. *Rev. Laser Eng.* **2008**, *36*, 1172. [[CrossRef](#)]
19. Gaul, E.; Cheriaux, G.; Antipenkov, R.; Batysta, F.; Borger, T.; Friedman, G.; Greene, J.T.; Hammond, D.; Heisler, J.; Hidingier, D.; et al. Hybrid OPCPA/Glass 10 PW laser at 1 shot a minute. In Proceedings of the Conference on Lasers and Electro-Optics, San Jose, CA, USA, 13–18 May 2018.
20. Gaul, E.W.; Martinez, M.; Blakeney, J.; Jochmann, A.; Ringuette, M.; Hammond, D.; Borger, T.; Escamilla, R.; Douglas, S.; Henderson, W.; et al. Demonstration of a 1.1 petawatt laser based on a hybrid optical parametric chirped pulse amplification/mixed Nd:glass amplifier. *Appl. Opt.* **2010**, *49*, 1676. [[CrossRef](#)] [[PubMed](#)]
21. Cheriaux, G.; Antipenkov, R.; Batysta, F.; Borger, T.; Friedman, G.; Greene, J.T.; Hammond, D.; Heisler, J.; Jochmann, A.; Kepler, M.; et al. Progress on ELI-Beamlines 10 PW Laser System. *Rev. Laser Eng.* **2018**, *46*, 125. [[CrossRef](#)]
22. Zhang, Z.; Song, Y.; Sun, D.; Chai, L.; Sun, H.; Wang, C. Compact and material-dispersion-compatible Offner stretcher for chirped pulse amplifications. *Opt. Commun.* **2002**, *206*, 7. [[CrossRef](#)]
23. Heebner, J.E.; Acree, R.J.; Alessi, D.A.; Barnes, A.I.; Bowers, M.W.; Browning, D.F.; Budge, T.S.; Burns, S.; Chang, L.S.; Christensen, K.S.; et al. Injection laser system for Advanced Radiographic Capability using chirped pulse amplification on the National Ignition Facility. *Appl. Opt.* **2019**, *58*, 8501. [[CrossRef](#)] [[PubMed](#)]
24. Zhang, T.; Li, D.; Wang, T.; Cui, Y.; Zhang, T.; Wang, L.; Zhang, J.; Xu, G. Spectral shaping of picosecond petawatt laser system based on lithium niobate birefringent crystal. *Acta Phys. Sin.* **2021**, *70*, 084202. [[CrossRef](#)]
25. Preuss, D.R.; Gole, J.L. Three-stage birefringent filter tuning smoothly over the visible region: Theoretical treatment and experimental design. *Appl. Opt.* **1980**, *19*, 702. [[CrossRef](#)] [[PubMed](#)]
26. Zhu, X. Explicit Jones transformation matrix for a tilted birefringent plate with its optic axis parallel to the plate surface. *Appl. Opt.* **1994**, *33*, 3502. [[CrossRef](#)]
27. Burneau, A.; Humbert, B. Temperature effect on a tilted birefringent filter in a tunable laser: A limitation for Raman spectroscopy. *J. Appl. Phys.* **1989**, *66*, 5702. [[CrossRef](#)]
28. Batysta, F.; Antipenkov, R.; Borger, T.; Kissinger, A.; Green, J.T.; Kananavicius, R.; Cheriaux, G.; Hidingier, D.; Kolenda, J.; Gaul, E.; et al. Spectral pulse shaping of a 5 Hz, multi-joule, broadband optical parametric chirped pulse amplification frontend for a 10 PW laser system. *Opt. Lett.* **2018**, *43*, 3866. [[CrossRef](#)]
29. Zhang, Z.; Sun, H. Calculation and evaluation of dispersions in a femtosecond pulse amplification system. *Acta Phys. Sin.* **2001**, *50*, 1080. [[CrossRef](#)]
30. Tian, J.; Sun, J.; Wei, Z.; Wang, Z.; Ling, W.; Huang, X.; Liu, L.; Wei, X.; Zhang, J. Theoretical and experimental studies on large-ratio stretching of femtosecond pulse with Offner triplet stretcher. *Acta Phys. Sin.* **2005**, *54*, 1200. [[CrossRef](#)]
31. Treacy, E. Optical pulse compression with diffraction gratings. *IEEE JQE* **1969**, *5*, 454. [[CrossRef](#)]
32. Liu, X.; Wang, C.; Wang, X.; Lu, X.; Bai, P.; Liu, Y.; Li, Y.; Liu, K.; Yu, L.; Leng, Y.; et al. Dispersion Management in 10-PW Laser Front End. *Optics* **2020**, *1*, 191–201. [[CrossRef](#)]
33. Brown, M. Increased spectral bandwidths in nonlinear conversion processes by use of multicrystal designs. *Opt. Lett.* **1998**, *23*, 1591. [[CrossRef](#)] [[PubMed](#)]